

Fluid flocks with inertia

Rayan Chatterjee,¹ Navdeep Rana,¹ R. Aditi Simha,^{2,*} Prasad Perlekar,¹ and Sriram Ramaswamy³

¹Tata Institute of Fundamental Research, Centre for Interdisciplinary Sciences, Hyderabad 500 107, India

²Department of Physics, Indian Institute Of Technology Madras, Chennai 600 036, India

³Centre for Condensed Matter Theory, Department of Physics,
Indian Institute of Science, Bangalore 560 012, India

Inertia drives a flocking transition in extensile active suspensions. In a system with mass density ρ , viscosity μ , mean active stress σ_0 , characteristic self-propulsion speed v_0 , Frank elastic constant K and flow-alignment parameter λ , a state with macroscopically aligned direction of self-propulsion displays two linear instabilities governed by the dimensionless combination $R \equiv \rho v_0^2 / 2\sigma_0$. For $R < R_1 = 1 + \lambda$ disturbances at small wavenumber q grow at a rate $q[(R_1 - R)\sigma_0/2\rho]^{1/2}$, which can be viewed as the inertial continuation of the Stokesian instability [PRL **89**, 058101 (2002)] of active liquid crystals. The resulting statistical steady state is found numerically to be isotropic hedgehog-defect turbulence. For $R_1 < R < R_2 \simeq \mu^2 R_1 / 4K\rho$ a distinct linear instability arises, with growth rate $\sim q^2|R - R_1|^{-1/2}\mu/\rho$ for $R \rightarrow R_1$ and $\sim q^2|R - R_2|\mu/\rho$ for $R \rightarrow R_2$. Direct numerical solution in the parameter range of this $O(q^2)$ instability however reveals a *phase-turbulent* but *aligned* state. $R = R_1$ thus marks an inertia-driven phase transition from the statistically isotropic phase to a noisy but ordered flock. We present numerical evidence in three and two dimensions for continuous order-parameter onset and a growing correlation length of fluctuations upon approaching the transition. Linear stability analysis and direct numerical solution agree that the dominant instability mode for extensile systems is twist, which is three-dimensional; contractile systems fail two-dimensionally. We highlight striking statistical differences between the resulting turbulent states. Finally, for $R > R_2$, a state of polar uniaxial alignment is *stable* to small perturbations at *all* wavenumbers q .

I. INTRODUCTION

The theory of active matter [1–3] is the framework of choice for understanding the collective behaviour of motile particles. A familiar example of self-organization in active systems is flocking [4–6] – *polar* orientational order, with a *vector* order parameter characterizing the degree to which the constituents point and move in a common direction. The other common type of uniaxial order, well-known from liquid crystals, is *apolar* or *nematic*: spontaneous alignment with an axis but no fore-aft distinction, encoded in a traceless symmetric *tensor* order parameter. Similarly, it is natural to consider two ideal dynamical regimes [2]: *wet*, i.e., suspended in unbounded bulk fluid so that Galilean invariance and momentum conservation hold sway, and *dry*, where the active particles are typically in contact with a solid substrate which offers a preferred frame of reference, and whose internal dynamics we approximate by the damping and noise of a momentum sink. Microfluidic experiments on suspensions of active particles define a third “confined wet” [2] domain where motion is limited to one or two dimensions by momentum-absorbing walls but the fluid still exerts a long-range influence through the constraint of incompressibility. Unlike at thermal equilibrium, the steady-state phase diagrams of active systems are sensitive to which of these distinct dynamical ensembles is imposed.

Purely viscous aligned wet active matter in bulk is unstable without threshold [7]. In a finite geometry such as

a channel, or on a substrate, the instability manifests itself as an active variant [8] of the Fréedericksz [9, 10] transition, with an onset threshold that scales to zero with increasing channel width or decreasing substrate friction. The instability and the ensuing spontaneous flow [8] and defect proliferation are widely observed [11–26] and lie at the heart of “bacterial turbulence” [3, 17, 27–31]. This Stokesian instability can be understood by considering uniaxial active stresses within an *apolar* description [32].

Stable flocks in bulk fluid are, however, widely observed in the form of fish schools, which are far from Stokesian and overwhelmingly polar. Can our local hydrodynamic framework account for their stability? Only a limited early result [7] is available: when inertia, that is unsteadiness, is taken into account, a parameter domain exists over which the dynamic response of polar flocks in fluid, to first order in small wavenumbers q , is wavelike, that is, oscillatory rather than growing or decaying. Existing studies of self-propulsion at modest but nonzero Reynolds number examine, inter alia, pusher-puller differences in stability and efficiency [33] and hydrodynamic interaction [34, 35], and velocity reversal with frequency [36] in oscillating sphere-dimer swimmers [37, 38]. A phase diagram featuring fluid flocks as active liquid crystals, with inertial effects included, is to our knowledge unavailable.

In this article we examine the combined effects of fluid inertia and polarity, i.e., fore-aft asymmetry, and the distinctive characteristics of three-dimensional perturbations, on the dynamics of an incompressible active suspension in a state of *vectorial* orientational order, characterized by a self-propelling speed v_0 , a scale σ_0 of active stress, shear viscosity μ , a single Frank elastic constant

* deceased

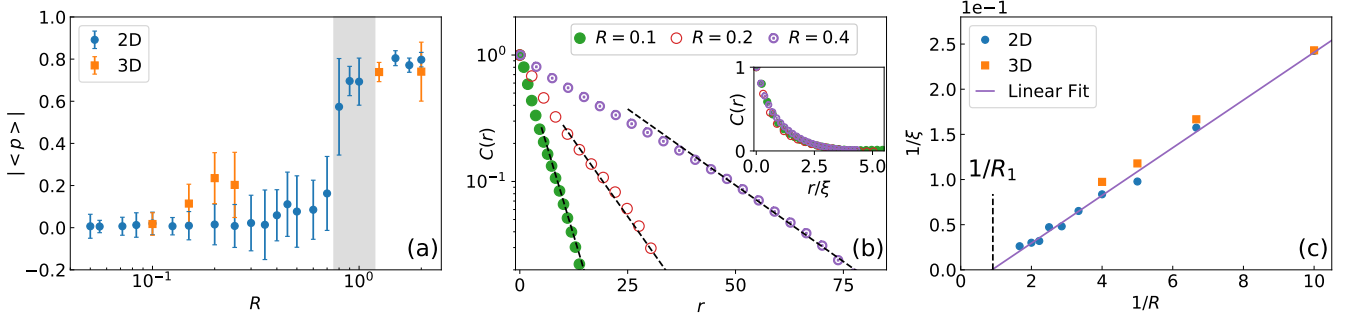


FIG. 1. (a) Variation of the order parameter $|\langle \mathbf{p} \rangle|$ with R for our 2D and 3D simulations (see Table I), with the shaded region indicating the transition regime around $R = R_1$ as predicted by the linear stability analysis. For each of the data point, the spatio-temporal average is calculated from ~ 80 statistically independent realizations and the unit standard deviation about the average is shown as the error-bar. (b) Semilog plot of the correlation function $C(r)$ versus r for $R = 0.1, 0.2$, and 0.4 ($R < R_1$, run SPP4). The dashed line indicate the exponential fit. Inset: Collapse of steady state longitudinal correlation function (LCF) when distance is scaled with the correlation length. (c) Plot of inverse correlation length $1/\xi$ versus $1/R$. Continuous purple line shows the linear fit to 2D data. Note that from the intercept of the linear fit on the horizontal axis we conclude that the correlation length diverges around $R \approx R_1$.

K , and total mass density ρ . In order to highlight intrinsic chaotic properties, we do not add noise to our equations. Our results are most accessibly presented in the limit in which the polar nature of the system is encoded only in self-advection of the polar order parameter, with other polar terms set to zero. We summarise them here [see Fig. (1)].

- For $\sigma_0 > 0$, the “pusher” or “extensile” case of Stokesian active hydrodynamics [7, 8, 39], the dimensionless combination

$$R \equiv \rho v_0^2 / 2\sigma_0, \quad (1)$$

which compares inertial effects of self-propulsion to active stresses, governs the dynamics of a polar fluid flock. Qualitative changes in behaviour as function of R take place across two thresholds, $R = R_1 = 1 + \lambda$, where λ is a flow-coupling parameter, and $R = R_2 \simeq R_1(1 + \beta)^2 / 4\beta$ where

$$\beta = \Gamma K \rho / \mu, \quad (2)$$

Γ being an orientational mobility. We expect $\Gamma \sim 1/\mu$, so β is expected to be of the same order of magnitude as

$$\alpha = K \rho / \mu^2 \quad (3)$$

$R_2 \geq R_1$ for all β , with equality for $\beta = 1$. If $\beta \simeq \alpha \ll 1$, as is the case for molecular liquid crystals [40], then $R_2 \gg R_1$.

- For $R < R_1$ disturbances at small wavevector q along the ordering direction grow at a rate $q\sqrt{(R_1 - R)\sigma_0/2\rho}$, connecting at larger q to the Stokesian instability [7] of active liquid crystals. The result of this instability on long timescales, we show numerically, is a turbulent state dominated by hedgehog defects.

- For $R_1 < R < R_2$ the state of uniform alignment is still linearly unstable, but $q^2(\mu/\rho)[(1 - \beta)(1 - R_1/R)^{-1/2} - (1 + \beta)]$. We find by direct numerical solution that nonlinearities limit the effect of this $O(q^2)$ instability, and the system remains in a *phase-turbulent* but *aligned* state. Thus at $R = R_1$ the system undergoes a nonequilibrium phase transition, driven by inertia, from a statistically isotropic defect-turbulent phase to a noisy but ordered flock.
- Our numerical studies find evidence for a continuous onset of the polar order parameter as R increases past R_1 , and a substantial growth of the correlation length of fluctuations upon approaching the transition.
- For $R > R_2$ the flock outruns the instability: small fluctuations decay at all wavevectors. Note however that in practice R_2 could be very large, as it goes to ∞ both for $\beta \rightarrow 0$ and $\beta \rightarrow \infty$.
- The regime of the $O(q^2)$ instability is completely eliminated in the special limit $\beta = 1$, which corresponds to equal diffusivities for velocity gradients and director distortions. This limit corresponds to setting the Frank constant K equal to Purcell’s [41] critical viscous force μ^2/ρ , inconceivable for equilibrium molecular systems [40] but not ruled out *a priori* for flocks.
- Contractile suspensions, $\sigma_0 < 0$, remain unstable even in presence of inertia ρ and motility v_0 ; disturbances with q normal to the ordering direction have small- q growth rate $\sim q\sqrt{|\sigma_0|(1 + \lambda)/\rho}$.
- The instability modes for extensile systems are typically three-dimensional, provoking twist as well as

bend, whereas for contractile systems, the characteristic failure mode is splay, which is two-dimensional.

Testing our predictions requires the creation of experimental systems in which stable flocks in fluid at moderate Reynolds number, and their order-disorder phase transition, can be studied in a well-controlled manner. Our findings thus open an unexplored direction in active matter.

The remainder of this article is organised as follows. In § II we present the governing equations for polar active suspensions and investigate the linear stability of the uniaxially ordered state. In § III, using high-resolution direct numerical simulation (DNS), we investigate both the short-time growth of perturbation amplitudes, which we compare to the linear stability analysis, and the long-time stationary states of our system. Within the DNS we vary R to uncover a nonequilibrium phase transition from defect turbulence to phase turbulence, and measure order-parameter onset, correlation functions, topological

defects and power spectra. Finally, in § IV we present a summary and projections for the future.

II. GOVERNING EQUATIONS AND STABILITY ANALYSIS

A. Hydrodynamics of active suspensions

We begin by recalling for the reader the equations of motion for the hydrodynamic velocity field \mathbf{u} , the polar order parameter field \mathbf{p} , and the active particle concentration c , as functions of position \mathbf{r} and time t , for bulk active suspensions [7]. Note that \mathbf{p} is not the nematic director [10], and not a unit vector: its magnitude measures the degree of polar, i.e., vectorial, order, and $\mathbf{p} \rightarrow -\mathbf{p}$ is not a symmetry unless \mathbf{r} and \mathbf{u} are reversed as well. At this stage we therefore include for completeness all leading-order polar terms [2, 42–44]. The equations are:

$$\rho(\partial_t \mathbf{u} + \mathbf{u} \cdot \nabla \mathbf{u}) = -\nabla P + \mu \nabla^2 \mathbf{u} + \nabla \cdot (\boldsymbol{\Sigma}^a + \boldsymbol{\Sigma}^r), \quad (4)$$

$$\partial_t \mathbf{p} + (\mathbf{u} + v_0 \mathbf{p}) \cdot \nabla \mathbf{p} = \lambda \mathbf{S} \cdot \mathbf{p} + \boldsymbol{\Omega} \cdot \mathbf{p} + \Gamma \mathbf{h} + \ell \nabla^2 \mathbf{u}, \text{ and} \quad (5)$$

$$\partial_t c + \nabla \cdot [(\mathbf{u} + v_1 \mathbf{p})c] = 0. \quad (6)$$

Here, the hydrodynamic pressure P enforces incompressibility $\nabla \cdot \mathbf{u} = 0$, \mathbf{S} and $\boldsymbol{\Omega}$ are the symmetric and anti-symmetric parts of the velocity gradient tensor $\nabla \mathbf{u}$, and

$$\boldsymbol{\Sigma}^a \equiv \sigma_a(c) \mathbf{p} \mathbf{p} - \gamma \nabla \mathbf{p} - \bar{\gamma} \nabla \mathbf{p}^T \quad (7)$$

is the intrinsic stress associated with swimming activity, where $\sigma_a > (<)0$ for extensile (contractile) swimmers [2, 7] is the familiar force-dipole density. We use it here to describe the flow fields created by force-free motion even when suspension inertia is included. In Eqs. (4)–(7), the superscript T denotes matrix transpose, and $\gamma, \bar{\gamma}$, with units of surface tension and presumably of order σ_0 times an active-particle size, control the lowest-order *polar* contribution to the active stress. In principle all parameters should be functions of the local concentration c ; we have made this dependence explicit in the case of σ_a . We further define the mean strength of active stress

$$\sigma_0 \equiv \sigma_a(c_0), \quad (8)$$

where c_0 is the mean concentration.

$$\boldsymbol{\Sigma}^r = \frac{\lambda+1}{2} \mathbf{h} \mathbf{p} + \frac{\lambda-1}{2} \mathbf{p} \mathbf{h} - \ell \nabla \mathbf{h} - \bar{\ell} \nabla \mathbf{h}^T \quad (9)$$

is the reversible thermodynamic stress [45], $\mathbf{h} = -\delta F / \delta \mathbf{p}$ is the molecular field conjugate to \mathbf{p} , derived from a free-energy functional

$$F = \int d^3 r [(1/4)(\mathbf{p} \cdot \mathbf{p} - 1)^2 + (K/2)(\nabla \mathbf{p})^2 - E \mathbf{p} \cdot \nabla c] \quad (10)$$

favouring a \mathbf{p} -field of uniform unit magnitude [46] which we have rescaled to unity in Eq. (10). A Frank constant [47–49] K penalizes gradients in \mathbf{p} , and E promotes alignment of \mathbf{p} up or down gradients of c , according to its sign. μ is the shear viscosity of the suspension, and Γ , dimensionally an inverse viscosity and therefore expected to be of order $1/\mu$, is a collective rotational mobility for the relaxation of the polar order parameter field. λ is the conventional nematic flow-alignment parameter [50, 51] and $\ell, \bar{\ell}$, with units of length, govern the lowest-order *polar* flow-coupling term [44, 52, 53]. For simplicity of analysis, we will present results for $|\lambda| < 1$ unless otherwise stated. Polarity enters through the speeds v_0 and v_1 with which \mathbf{p} advects itself and the concentration respectively, the coefficients γ_{\pm} in the polar part of the stress in Eq. (7), and the polar flow-coupling length-scale ℓ . v_1 will drop out of our analysis as we will ignore the concentration field. To keep the analysis simple, and without any loss of essential physics, we set $\gamma, \bar{\gamma}, \ell$ and $\bar{\ell}$ to zero. These quantities enter a more detailed analysis through the dimensionless combinations $\mu v_0 / \gamma$ and $K / \sigma_0 \ell^2$ and the corresponding “barred” quantities; the present treatment sets these to infinity. Polar effects are then carried locally by v_0 alone. The vector nature of the order parameter will of course also be reflected globally in the nature of the allowed topological defects. Crucially, v_0 and σ_0 are independent quantities in our coarse-grained treatment, a point we will return to later in the paper.

We remind the reader that Eqs. (4) to (6) constitute a symmetry-based effective description on length-scales much larger than a fish (as we shall call our self-propelled particles hereafter). The viscosity μ and other parameters are coarse-grained properties of this active suspension which we treat as phenomenological coefficients, not to be confused with the corresponding quantities entering a near-equilibrium hydrodynamic description of the ambient fluid. We do not attempt to estimate their magnitudes, which no doubt receive “eddy” contributions from flows on scales of a few fish. Our approach is applicable even if some interactions such the aligning tendency are partly or wholly behavioural rather than mechanical, as long as they are local in space and time.

B. Linear Stability analysis

Defining the ordering direction to be $\hat{\mathbf{x}}$ and directions in the yz plane as \perp , we have investigated the stability of a uniform ordered flock ($c = c_0$, $\mathbf{u} = \mathbf{0}$, and $\mathbf{p} = \hat{\mathbf{x}}$, which is a stationary solution of Eqs.(4) - (6) to small perturbations ($\delta\mathbf{u}_\perp, \delta\mathbf{p}_\perp, \delta c$), where the presence of only

the \perp components is a result of incompressibility and the “fast” nature of p_x . We present here the results for the case where the concentration field c is removed from the analysis. This is sufficient for our purposes, because c does not participate significantly in the linear instabilities of relevance, as we now argue. Taking the curl with respect to ∇_\perp eliminates c from the \perp component of Eq. (5). A similar curl removes it from Eq. (4) as well, for \mathbf{q} purely along or purely normal to $\hat{\mathbf{x}}$. Thus, it does not participate in the dynamics of pure bend or twist. Taking the divergence of Eqs. (4) and (5) with respect to ∇_\perp reveals that c is present in the linearized dynamics only when $q_x \neq 0$, and is thus unimportant for considerations of pure splay. The removal of the concentration can be formalized by introducing birth and death of particles so that c becomes “fast” [54] and can be eliminated in favour of the slow variables \mathbf{p}_\perp and \mathbf{u}_\perp . We have checked (see Appendix) that the results from the linear stability analysis are qualitatively unaltered upon including the concentration. Defining the projector

$$\mathbf{T}_q \equiv \mathbf{I} - \hat{\mathbf{q}}\hat{\mathbf{q}} \quad (11)$$

transverse to \mathbf{q} and linearizing Eqs. (4) and (5) about the ordered state we find

$$(\rho\partial_t + \mu q^2) \delta\mathbf{u}_{\perp\mathbf{q}} = -i\mathbf{T}_q \cdot \left[\left(\sigma_0 + \frac{\lambda-1}{2} K q^2 \right) \hat{\mathbf{x}}\mathbf{q}_\perp + q_x \left(\sigma_0 + \frac{\lambda+1}{2} K q^2 \right) \mathbf{I} \right] \cdot \delta\mathbf{p}_{\perp\mathbf{q}} \quad (12)$$

$$\partial_t \delta\mathbf{p}_{\perp\mathbf{q}} = +i \left(\frac{\lambda+1}{2} q_x \mathbf{I} - \frac{\lambda-1}{2} \frac{\mathbf{q}_\perp \mathbf{q}_\perp}{q_x} \right) \cdot \delta\mathbf{u}_{\perp\mathbf{q}} - (i v_0 q_x + \Gamma K q^2) \delta\mathbf{p}_{\perp\mathbf{q}} \quad (13)$$

where σ_0 is $\sigma_a(c)$ evaluated at the mean concentration c_0 . As in [7], the divergence and curl of Eqs. (12) and (13) describe respectively the dynamics of splay and twist, with an admixture of bend in each case for $q_x \neq 0$. Defining ϕ

to be the angle between the wavevector \mathbf{q} and the alignment ($\hat{\mathbf{x}}$) direction, the resulting dispersion relations for the frequency ω , valid for all \mathbf{q} , for modes of the form $e^{i(\mathbf{q}\cdot\mathbf{r} - \omega t)}$, are

$$\omega = \omega_\pm^s = \frac{1}{2} v_0 q \cos \phi - i \frac{\mu_\pm}{2\rho} q^2 \pm \left(\frac{\sigma_0}{2\rho} \right)^{1/2} [A(\phi) q^2 + 2iB(\phi) q^3 + G(\phi) q^4]^{1/2} \quad (14)$$

for the splay-bend modes and

$$\omega_\pm^t = \frac{1}{2} v_0 q \cos \phi - i \frac{\mu_\pm}{2\rho} q^2 \pm \left(\frac{\sigma_0}{2\rho} \right)^{1/2} [A(0) \cos^2 \phi q^2 + 2iB(0) \cos \phi q^3 + \bar{G}(\phi) q^4]^{1/2} \quad (15)$$

for the twist-bend modes.

In Eqs. (14) and (15) we have defined

$$A(\phi) = R \cos^2 \phi - \cos 2\phi (1 + \lambda \cos 2\phi), \quad (16)$$

where $R \equiv \rho v_0^2 / 2\sigma_0$ was defined in Eqs. (1), $B(\phi) = (v_0 \mu_- / \sigma_0) \cos \phi$, $G(\phi) = -(\mu_-^2 / 2\rho \sigma_0) + (K/2\sigma_0)(1 + \lambda \cos 2\phi)^2$, and $\bar{G}(\phi) = -(\mu_-^2 / 2\rho \sigma_0) + (K/2\sigma_0)(1 +$

$\lambda)^2 \cos^2 \phi$ [55] where

$$\mu_\pm = \mu(1 \pm \beta), \quad (17)$$

with β as defined in (2), which should be of the same order as α defined in Eq. (3) assuming $\Gamma \sim 1/\mu$. For conventional liquid crystals therefore $\beta \ll 1$ as well.

Even before examining the asymptotic small- or large- q behaviour, we can read off the effects of competition between the inertia of motility and active stress, through the crucial parameter R defined in Eq. (1). From Eqs. (14) and (15) instabilities driven by active stress clearly operate through a large negative $A(\phi)$, and a sufficiently large R can keep $A(\phi)$ positive. It is also clear that the contribution of R vanishes for pure splay, Eq. (14) at $\phi = \pi/2$, so motility cannot stabilize contractile ($\sigma_0 < 0$) flocks in fluid against the splay instability. In the remainder of this section we therefore discuss the stabilizing influence of the inertia of self-propulsion on extensile ($\sigma_0 > 0$) systems. We will return to the contractile case when we discuss active turbulence.

1. Small- q behaviour: the $O(q)$ and $O(q^2)$ instabilities

Let us first examine the small- q behaviour. Expanding Eqs. (14) and (15) up to order q^2 we then find

$$\omega = \omega_{\pm}^s = \frac{q}{2} \left\{ v_0 \cos \phi \pm \left[\frac{2\sigma_0}{\rho} A(\phi) \right]^{1/2} \right\} - \frac{i}{2} \frac{\mu}{\rho} q^2 \left\{ 1 + \beta \mp (1 - \beta) \left[\frac{R \cos^2 \phi}{A(\phi)} \right]^{1/2} \right\} \quad (18)$$

for the splay-bend modes and

$$\omega = \omega_{\pm}^t = \frac{q}{2} \cos \phi \left\{ v_0 \pm \left[\frac{2\sigma_0}{\rho} A(0) \right]^{1/2} \right\} - \frac{i}{2} \frac{\mu}{\rho} q^2 \left\{ 1 + \beta \mp (1 - \beta) \left[\frac{R}{A(0)} \right]^{1/2} \right\} \quad (19)$$

for the twist-bend modes. Here $A(\phi)$ was defined in Eq. (16) and $A(0) = A(\phi = 0) = R - (1 + \lambda)$. One note of caution: the small- q expansion that led to Eq. (19) assumes $v_0 q \cos \phi > q^2 \mu / \rho$, which means that it does not apply for $\phi = \pi/2$, i.e., pure twist. It does however hold for any $\phi \in [0, \pi/2)$ but the closer ϕ is to $\pi/2$ the smaller q must be for the result to apply.

Two of our main results now follow. If $R < 1 + \lambda$, Eq. (19) signals a bend instability with small- q growth rate $\sim q$. This was discussed in the strictly apolar case $v_0 = 0$ in [7], and can be viewed as the small- q extension of the Stokesian bend instability [7]. However, if $R > 1 + \lambda$, so that the $O(q)$ instability is averted, $0 < 1 - (1 + \lambda)/R < 1$. If R is not too large, this means the coefficient

of iq^2 in Eqs. (18) and (19) is positive, signalling a small- q instability with *diffusive* growth. This $O(q^2)$ instability exists for R between $R_1 = 1 + \lambda$ and

$$R_2 = \frac{\mu_+^2}{\mu_+^2 - \mu_-^2} R_1 = \frac{1 + \lambda}{4\beta} (1 + \beta)^2. \quad (20)$$

For $R > R_2$ the flock is linearly stable. If $\beta \ll 1$ as in molecular systems, $R_2 \gg R_1$, and the $O(q^2)$ instability occupies a large range of R . In the $\beta = 0$ limit the uniformly ordered flock is *always* linearly unstable, with small- q growth rate $\sim q$ for $R < 1 + \lambda$ and $\sim q^2$ for $R > 1 + \lambda$.

Note that the $O(q^2)$ instability can be eliminated in the special case $\beta = 1$, i.e., $\mu/\rho = \Gamma K$. Noting that Γ should be roughly $1/\mu$, this condition implies $K = \mu^2/\rho$, an interesting condition that equates a Frank constant (which, recall, has units of force in three dimensions) to Purcell's intrinsic three-dimensional force scale [41] μ^2/ρ for viscous fluids. As we remarked above, β in molecular or colloidal systems is about 10^{-4} [10, 40], so requiring it to be order unity amounts to insisting that the fish have an exceptionally strong aligning interaction. This possibility cannot be ruled out a priori as alignment in living systems is likely to be active and behavioural, not a passive mechanical torque.

2. Large- q dynamics and the Stokesian limit

In order to relate the instabilities discussed above to the well-known Stokesian instability of aligned active suspensions, we define the lengths

$$\ell_v \equiv \mu/v_0\rho \text{ and } \ell_\sigma \equiv \mu/\sqrt{\rho\sigma_0} = R^{1/2}\ell_v \quad (21)$$

below which viscosity overwhelms the inertial effects of self-propulsion and

$$\ell_K \equiv \sqrt{K/\sigma_0} \quad (22)$$

below which Frank elasticity dominates active stresses. Note that

$$\frac{\ell_K}{\ell_v} = \sqrt{\alpha R} \quad (23)$$

can change substantially as R is varied. Expanding Eqs. (14) and (15) for $q \gg \max(\ell_v^{-1}, \ell_\sigma^{-1})$, we find, to leading order in α and β , that the splay-bend mode that goes unstable at small R has the form

$$\omega^s = -i \frac{\sigma_0}{2\mu} A(\phi) + v_0 q \cos \phi - i \left[\Gamma \mu + \frac{1}{4} (1 + \lambda \cos 2\phi)^2 \right] \frac{K}{\mu} q^2. \quad (24)$$

and the corresponding twist-bend mode has frequency

$$\omega^t = -i \frac{\sigma_0}{2\mu} A(0) \cos^2 \phi + v_0 q \cos \phi - i \left[\Gamma \mu + \frac{1}{4} (1 + \lambda)^2 \cos^2 \phi \right] \frac{K}{\mu} q^2. \quad (25)$$

where $A(\phi)$ is as defined in Eq. (16).

Note that Eqs. (24) and (25) are not Stokesian expressions but short-wavelength limits of the linearized dynamics of a polar active suspension *with inertia*, which enters through R . We see in particular that the stability criteria in this large- q regime are identical to those for the $O(q)$ mode at small q . Thus a twist-bend instability, with a growth rate $\sim \sigma_0/\mu$ for $\max(\ell_v^{-1}, \ell_\sigma^{-1}) \ll q \ll \ell_K^{-1}$ takes place if $R < 1 + \lambda$. This establishes our claim that the $O(q)$ instability is the small- q extension of the Stokesian instability [7] of active suspensions. The $O(q^2)$ instability that intervenes at small q as R is increased does not reflect itself in the large- q dynamics.

It is important to keep in mind that the active stress σ_0 is a partial description of the mechanics of self-propulsion based on an estimate of the force-dipole concentration, and is not a priori determined by v_0 . To take an extreme case, Stokesian swimmers with no force dipole exist, e.g., the pure quadrupole [41, 56]. Assuming a volume fraction of order unity, let us nonetheless try to estimate R for typical swimmers of speed v_0 and size a (although we must remember that this size is notional in our coarse-grained description). For Reynolds number Re small at the scale of the individual organism it is plausible that $\sigma_0 \sim \mu v_0/a$. In that case $R \equiv \rho v_0^2/2\sigma_0 \sim \rho v_0 a/\mu = \text{Re} \ll 1$, so we can replace Eqs. (24) and (25) by their Stokesian approximations. For high- Re swimmers it is less obvious how to estimate σ_0 . If we take it still to be a viscous stress then $R = \text{Re}$ continues to hold, so now R dominates in Eqs. (24) and (25), or in Eqs. (14) and (15), guaranteeing stability. Even if $\sigma_0 \sim \rho v_0^2$, $R \sim 1$ and it is plausible that the instability is averted [57].

3. Dominance of twist in the three-dimensional instability

A noteworthy feature, to our knowledge not discussed in the literature, emerges in our three-dimensional analysis: there are two families of bend instability – mixed with splay as in Eqs. (18) and (24) and twist as in Eqs. (19) and (25). Interpolation with bend mitigates the instability in Eqs. (18) and (24), crossing over to stability for large enough ϕ , but twist in Eqs. (19) and (25) has no such effect. The twist-bend instability Eqs. (19) and (25) should thus dominate, as it occurs for all ϕ except precisely $\pi/2$. This abundance of twisted unstable modes in Eqs. (19) and (25), independent of the roles of polarity and inertia, is doubtless the explanation of the numerical observations of Shendruk *et al.* [58] in their study of three-dimensional extensile active nematics. Fig. 2 displays the growth or decay rates of the twist-bend mode as a function of wavenumber as R is varied. We now turn to a comprehensive numerical study of the dynamics in the various regimes defined by our linear stability analysis.

We summarise this section by noting that, when inertia is taken into account, orientable active suspensions can have two types of linear instability at small wavenumber q , governed by a control parameter R defined in

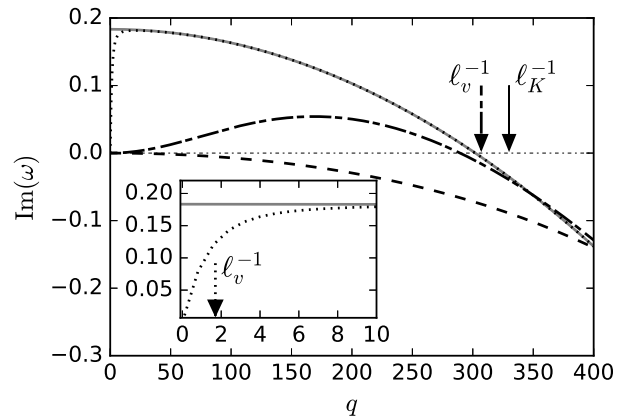


FIG. 2. Growth rate versus wavenumber. Gray line, Stokesian limit; black dotted line, $O(q)$ unstable, $\ell_v = 1$, $R = 5 \times 10^{-2}$; black dash-dotted, $O(q^2)$ unstable, $\ell_v = 3 \times 10^{-3}$, $R = 4.5 \times 10^3$; black dashed line, stable, $\ell_v = 3 \times 10^{-4}$, $R = 4.5 \times 10^5$. Arrows indicate wavenumber corresponding to ℓ_v for the unstable cases. For all the dispersion curves we use $\phi = 55^\circ$ and $K = 10^{-6}$ which sets $\ell_K = 3.2 \times 10^{-3}$.

Eq. (1). The instability growth-rates are of $O(q)$ for $R < R_1 = 1 + \lambda$ where λ is a flow-alignment parameter and $O(q^2)$ for $R_1 < R < R_2 \sim R_1/\beta$ where β is defined in Eq. (2). Linearly stable behaviour is found for $R > R_2$. As $\beta \sim 10^{-4}$ in molecular systems, the $O(q^2)$ -unstable regime occupies a rather large range in parameter space. Indeed one could argue that the typical behaviour is that corresponding to the $\beta = 0$ limit, in which the aligned state is always linearly unstable, either at $O(q)$ or at $O(q^2)$. In §III we gain insight beyond this linear analysis through a detailed numerical study to discover the long-time fate of the system in these unstable regimes.

III. NUMERICAL STUDIES OF ACTIVE HYDRODYNAMICS WITH INERTIA

In the following section we conduct a detailed set of simulations with varying R . We first verify the predictions of our linear stability analysis. Next, for extensile suspensions, we reveal an inertia-driven nonequilibrium phase transition from a disordered defect-turbulent state for $0 < R < R_1$ to an ordered phase-turbulent state for $R_1 \leq R < R_2$. We characterize these using the order parameter, correlation functions and energy spectrum.

A. Direct Numerical Simulations (DNS)

We numerically integrate Eqs. (4) and (5) in square and cubic domains of volume \mathcal{L}^d in dimensions $d = 2$ and 3. Spatial discretisation, with N^d collocation points, is

	D	\mathcal{L}	N	$v_0(\times 10^{-2})$	$K(\times 10^{-3})$	$R \equiv \rho v_0^2/2\sigma_0$
SPP1	3	2π	128	3.16	1	0.02, 0.0625
SPP2	3	10π	160	0.7, 13.4	2	0.01, 4
SPP3	3	10π	320	3.16	1	0.1 – 2
SPP4	2	20π	1024	3.16	1	0.05 – 2.0
SPP5	2	30π	1024	3.16	1	0.15, 0.20
SPP6	2	40π	2048	3.16	1	0.25, 0.30, 0.35
SPP7	2	60π	3072	3.16	1	0.4 – 0.6
SPP8	2	80π	4096	3.16	1	0.7

TABLE I. Spatial dimension D of the domain and parameters \mathcal{L} , N , ν , v_0 , K , and R used in our direct numerical simulations. The suspension density $\rho = 1$, $\lambda = 0.1$, $\mu = 0.1$ and the rotational mobility $\Gamma = 1$ are kept fixed for all the runs.

conducted by employing a pseudo-spectral method [59] for Eq. (4) and a fourth-order central finite-difference scheme for Eq. (5). For temporal integration we use a second-order Adams-Bashforth scheme [60]. Consistent with the linear stability analysis conducted earlier, we choose a uniform ordered state with transverse monochromatic perturbation as the initial condition, i.e. $\mathbf{u} = \mathbf{0} + A\hat{\mathbf{e}}_\perp \cos \mathbf{q} \cdot \mathbf{r}$, $\mathbf{p} = \hat{\mathbf{x}} + B\hat{\mathbf{e}}_\perp \cos \mathbf{q} \cdot \mathbf{r}$ where $\hat{\mathbf{e}}_\perp \equiv (\hat{\mathbf{y}} + \hat{\mathbf{z}})/\sqrt{2}$ is a unit vector in the plane perpendicular to the ordering direction, and we have made the arbitrary but acceptable choice $A = B = 10^{-3}$.

We monitor the time evolution of perturbations and, in the turbulent steady-state, investigate the statistical properties of the velocity and the director fields. In Table I, we summarize the parameters used in our DNS.

B. Initial growth of instabilities

We now present a comparison between the short-time growth obtained from the DNS with the analytical predictions of the linear stability analysis. The plot of the bend-twist dispersion curve given by Eq. (15) for $\phi = 55^\circ$ is shown in Fig. 3. The black dots indicate the the initial temporal growth rate of perturbations obtained from our DNS, which shows excellent agreement with the analytical results. Furthermore, our simulations correctly capture the exponential and oscillatory characters of the growth for $R < R_1$ and $R_1 < R < R_2$ respectively. Note that for $R < R_1$, the exponential growth rate of perturbations is much faster than the oscillatory kinematic contribution $\text{Re}[\omega] = v_0 q \cos \phi$. For $R_1 < R < R_2$, $\text{Re}[\omega]$ has contributions from both the kinematic and the inertial terms. Therefore, we observe an exponential growth of $|\mathbf{q}_\perp \times \delta \mathbf{p}_\perp|$ for $R < R_1$ [see Fig. (3A)], but oscillatory growth for $R_1 < R < R_2$ [see Fig. (3B)].

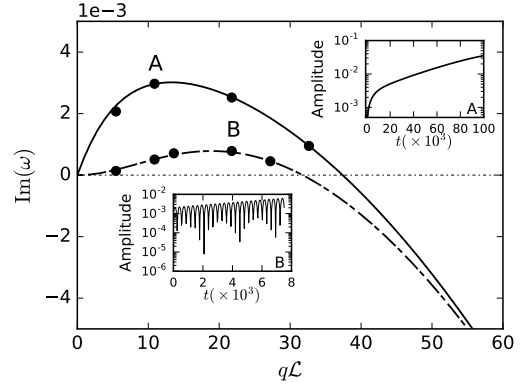


FIG. 3. Comparison of the growth rates obtained from dispersion relation Eq. (15) with those from DNS (black dots). (Inset) Initial time-evolution of the perturbation amplitude $|\mathbf{q}_\perp \times \delta \mathbf{p}_\perp|$ for $O(q)$: $R = 10^{-2}$ (A), and $O(q^2)$: $R = 4$ (B) growth rates (run SPP2). Note that we choose $\phi = 55^\circ$ for the initial perturbations.

C. A nonequilibrium phase transition

We now investigate the morphology and statistical properties of the orientation and flow emerging from the instabilities discussed above. Fig. (4) shows the typical flow structures observed in our DNS with increasing R in the statistically steady state. For $0 < R < R_1$, we observe hedgehog defects. The inter-defect spacing grows with increasing R . Unexpectedly, when R increases past the first threshold R_1 , a fluctuating but on average aligned state emerges. As we remarked in the Introduction, this is clear numerical evidence that $R = R_1$ marks a nonequilibrium phase transition from a statistically isotropic state to a flock or, in the terminology of spatiotemporal chaos, from defect turbulence to phase turbulence [61–63]. In the latter state long-wavelength statistical variation of the broken-symmetry variable is present but the amplitude of the order parameter is not destroyed by defects. We have not, however, measured the system-size dependence of the positive Lyapounov spectrum to establish spatiotemporal chaos quantitatively.

We now focus on the properties of the nonequilibrium phase transition. In Fig. 1(a), we plot the magnitude $|\langle \mathbf{p} \rangle|$ of the polar order parameter in the statistically steady state with increasing R , where angle brackets $\langle \cdot \rangle$ denote spatio-temporal averaging. For $R < R_1$, $|\langle \mathbf{p} \rangle|$ is consistent with zero. We observe an onset of polar order once R increases beyond $R_1 \equiv 1 + \lambda$. However, a detailed finite-size scaling analysis needs to be undertaken to find the correct scaling near the critical region. In the defect-turbulence regime, we study the steady-state longitudinal correlation function $C(r) = \langle \mathbf{p}_r(\mathbf{x}) \cdot \mathbf{p}_r(\mathbf{x} + \mathbf{r}) \rangle / \langle \mathbf{p}_r(0)^2 \rangle$, scaled to unity for $\mathbf{r} = \mathbf{0}$, where $\mathbf{p}_r = \mathbf{p} \cdot \hat{\mathbf{r}}$. We plot the correlation function $C(r)$ versus r in Fig. 1(b) and evaluate the correlation length by fitting an exponential

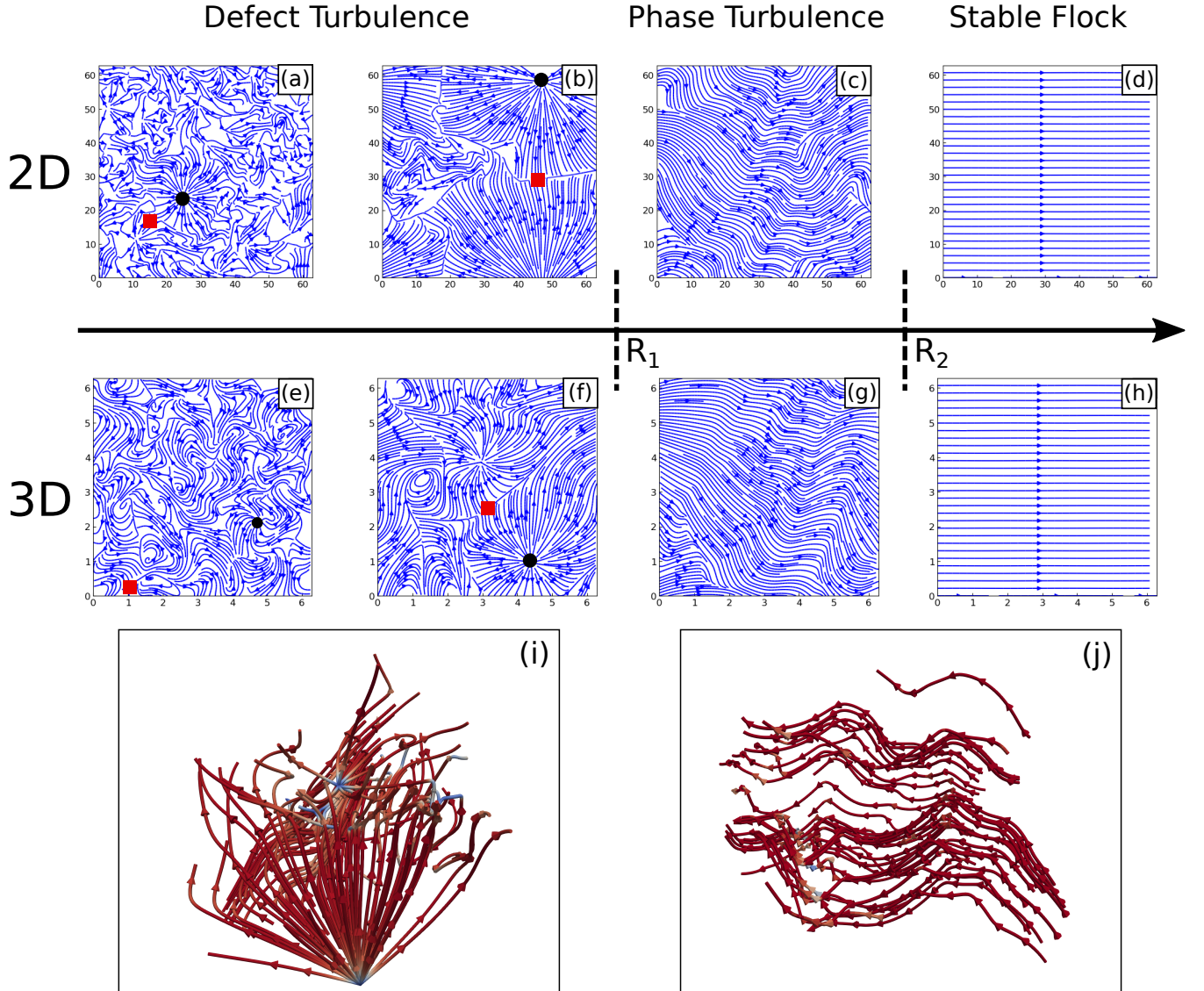


FIG. 4. Increasing inter-defect distance as function of R . Order parameter streamlines for 2D (run SPP4): (a) $R = 0.1$, (b) $R = 0.25$, (c) $R = 2$, and (d) $R > 12$; streamlines in $y = 0$ plane for 3D (runs SPP1 and SPP3): (e) $R = 0.02$, (f) $R = 0.0625$, (g) $R = 1.25$, and (h) $R > 12$. Typical hedgehogs are marked with filled black circles and red squares indicate saddles. (i) Zoomed in view of the three-dimensional order parameter streamlines showing the complex patterns between a hedgehog-saddle-hedgehog configuration in (f). (j) Three-dimensional nearly ordered configuration in the phase turbulence regime in (g).

decay $\exp(-r/\xi)$ to the tail of $C(r)$ [64]. We see that the correlation functions for different values of $R < R_1$ fall on a single curve plotted against r/ξ . Moreover, from Fig. 1(c), ξ grows and possibly diverges as $R \rightarrow R_1$; our limited data points are consistent with an exponent of unity.

D. Energy spectrum

Guided by the practice in hydrodynamic turbulence, we define the shell-averaged energy spectra

$$E_u(q) = \sum_{q-1/2 \leq \mathbf{m} < q+1/2} |\mathbf{u}_{\mathbf{m}}|^2, \text{ and}$$

$$E_p(q) = \sum_{q-1/2 \leq \mathbf{m} < q+1/2} |\mathbf{p}_{\mathbf{m}}|^2, \quad (26)$$

where $\mathbf{u}_{\mathbf{m}}$ and $\mathbf{p}_{\mathbf{m}}$ are the Fourier coefficients of the velocity \mathbf{u} and order parameter \mathbf{p} fields. The behaviours of

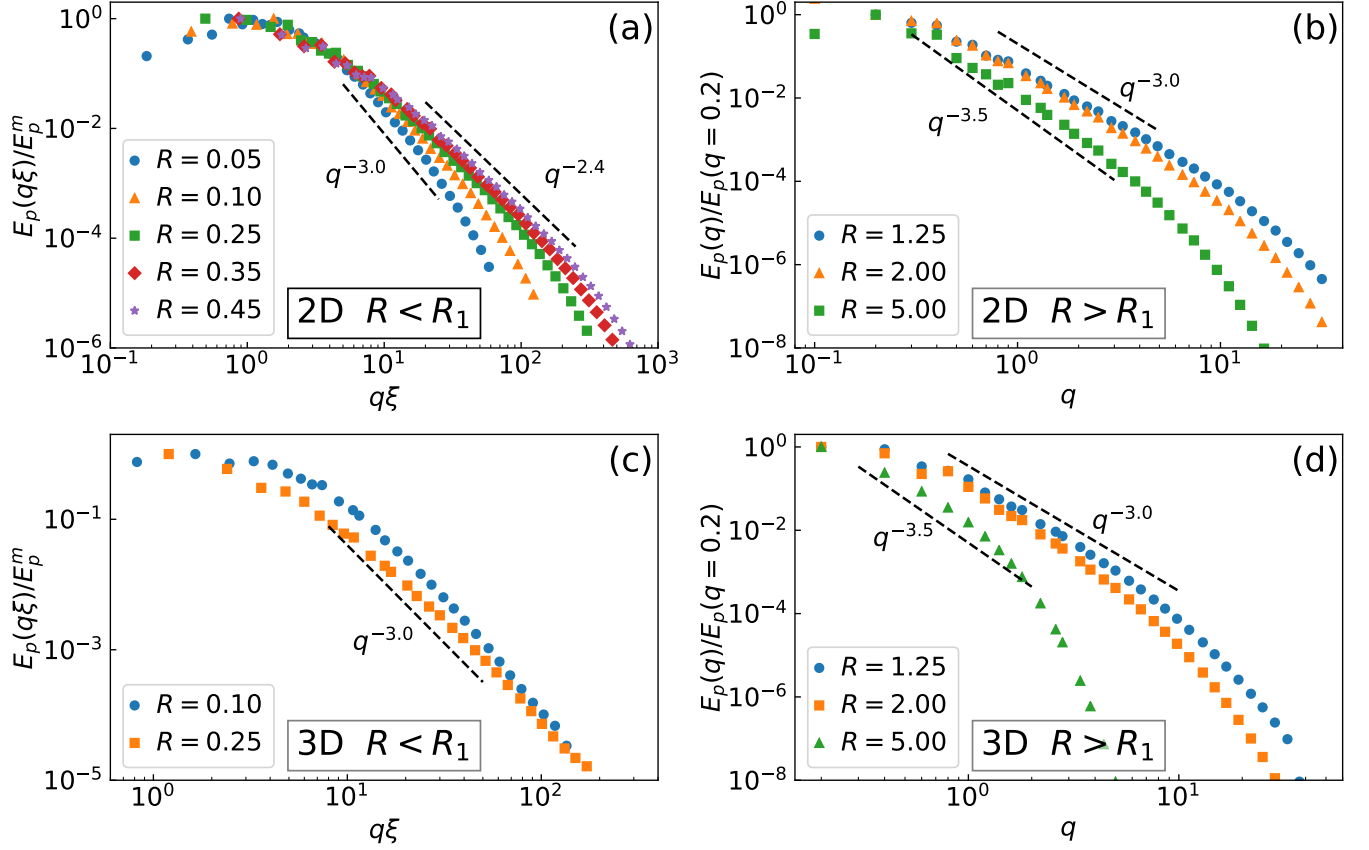


FIG. 5. Order parameter energy spectrum $E_p(q)$ for different values of R for (a,b) two-dimensional [runs SPP4] and (c,d) three-dimensional [runs SPP3] active suspension. For $R < R_1$ and $q\xi > 1$, we observe $E_p(q) \sim q^{-2.9}$ for small R and the slope marginally decreases to $q^{-2.4}$ as R approaches R_1 . For $R_1 < R < R_2$, $E_p(q) \sim q^{-3}$ for $R = 1.25$ and the slope increases to $q^{-3.5}$ for $R = 5$.

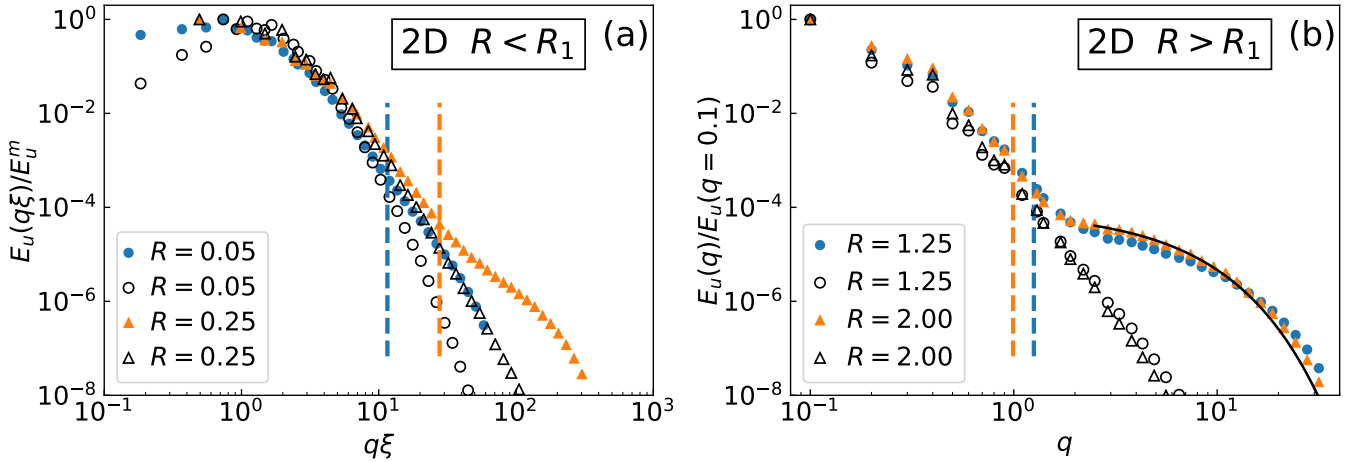


FIG. 6. Kinetic energy spectrum $E_u(q)$ for different values of R for 2D active suspension [runs SPP4] for $R < R_1$ (a) and $R > R_1$ (b). Similar to order parameter spectrum we observe power-law behavior for $1 < q\xi < q_\sigma\xi$, where $q_\sigma \equiv 2\pi/\ell_\sigma$. For small- q , we find a good agreement between the energy spectrum and the prediction $E_u(q) \sim [E_p(q)]^2$ (unfilled symbols). For $R > R_1$ and large- q ($q > q_\sigma$) the energy spectrum shows an exponential decay $E_u(q) \sim \exp(-0.29q)$ (black line). For different values of R , dashed vertical lines (with same color as markers) are drawn at $q = q_\sigma$.

$E_p(q)$ and $E_u(q)$ for a range of values of R are displayed in Figs. 5 and 6. We observe that for $R < R_1$, the spec-

trum peaks around $q\xi \sim 1$. For $q\xi > 1$, $E_p(q) \sim q^{-\Delta}$ with $\Delta = 3$. We observe a gradual decrease in the exponent Δ from 3 to 2.4 as R approaches R_1 . We emphasize that the quoted exponent values are empirically determined by conservatively selecting a dynamic range of wavenumbers away from the smallest $\sim 1/L$ and the largest, viz., $q_K \equiv 2\pi/\ell_K$ where elasticity dominates. In the phase-turbulence regime, $R_1 < R < R_2$, we observe $E_p(q) \sim q^{-3}$ for R close to R_1 . As R approaches R_2 , the effect of fluctuations decrease and we observe a systematic steepening of the slope (Δ).

In Eq. (4) we expect the dominant balance to be between acceleration and activity as the Reynolds number obtained by comparing the advective and viscous terms, based on the root-mean-square hydrodynamic velocity, is small ($\text{Re} \equiv \rho u_{rms}\xi/\mu \leq 0.5$) [65]. We therefore expect for small q , $\omega u_q \sim \sigma_0 q E_p(q)$. Using $\omega \sim v_0 q$ [see Eq. (14)] we get, $E_u(q) \sim (\sigma_0/v_0)^2 E_p(q)^2$. The plot in Fig. 6(a) shows good agreement between $E_u(q)$ obtained from our DNS and the prediction above for small q . For large $q > 2\pi/\ell_\sigma$, we expect viscous dissipation to be dominant and therefore, similar to dissipation range in hydrodynamic turbulence, we expect an exponential decay in the energy spectrum $E_u(q) \sim \exp(-ak^\delta)$ [66, 67]. From our numerical simulations, we find $\delta = 1$.

IV. SUMMARY AND PROSPECT

1. We have shown that inertia drives a nonequilibrium phase transition in polar active suspensions, from a defect-disordered state to an ordered and statistically stable flock. The governing control parameter R is the ratio of the inertial effects of self-propulsion to the scale of active stress as measured by the mean force-dipole density, and displays two thresholds R_1 , R_2 obtained from linear stability analysis. This dramatic advance in the theory of flocks in fluid, whose instability [7] can now be seen as simply the Stokesian limit of a rich phase diagram, should stimulate a new wave of experiments on swimmers at nonzero Reynolds number. The design of controlled experimental systems for this purpose is therefore an important challenge.
2. For $R < R_1$ we show a linear dependence of perturbation growth-rate on wavenumber q as $q \rightarrow 0$,

which connects smoothly at higher wavenumbers to the classical Stokesian instability [7] of active suspensions. The nonequilibrium steady state in this domain is a turbulence dominated by hedgehog-defects.

3. Linear instability persists for $R_1 < R < R_2$, which should cover most of the parameter space, because we expect $R_2 \gg R_1$, but the disturbance growth-rate at low wavenumbers is diffusive. Despite the instability, the final stationary state is an ordered, though noisy, flock.
4. We have characterized the phase transition from defect turbulence to phase turbulence by using standard tools from statistical mechanics, and find evidence for a continuous onset of order and a growing correlation length.
5. This phase transition is exclusively for *extensile* suspensions; we have shown that inertia cannot prevent the instability of *splay* distortions in *contractile* suspensions.
6. Finally we highlight the distinct role of three dimensional perturbations in the destabilization of extensile suspensions.

We look forward to tests of our theory in experiments and particle-based numerical simulations.

ACKNOWLEDGMENTS

SR was supported by a J C Bose Fellowship of the SERB (India) and the Tata Education and Development Trust. RC acknowledges the support of the SERB (India). RC, NR, PP and SR dedicate this article to the memory of Aditi Simha.

Appendix: Stability analysis with concentration

We now present the linear stability analysis in presence of the concentration field. Linearizing Eqs. (4), (5) and (6) about the base state ($\mathbf{u} = 0, \mathbf{p} = \hat{\mathbf{x}}, c = c_0$) we get:

$$(\rho\partial_t + \mu q^2) \delta \mathbf{u}_{\perp q} = -i\mathbf{T}_q \cdot \left[\left(\sigma_0 + \frac{\lambda-1}{2} K q^2 \right) \hat{\mathbf{x}} \mathbf{q}_{\perp} + q_x \left(\sigma_0 + \frac{\lambda+1}{2} K q^2 \right) \mathbf{l} \right] \cdot \delta \mathbf{p}_{\perp q} - i\mathbf{T}_q \cdot (\sigma_0 c_0 q_x \hat{\mathbf{x}}) \delta c_q, \quad (\text{A.1})$$

$$\partial_t \delta \mathbf{p}_{\perp q} = +i \left(\frac{\lambda+1}{2} q_x \mathbf{l} - \frac{\lambda-1}{2} \frac{\mathbf{q}_{\perp} \mathbf{q}_{\perp}}{q_x} \right) \cdot \delta \mathbf{u}_{\perp q} - (i v_0 q_x + \Gamma K q^2) \delta \mathbf{p}_{\perp q} + i \mathbf{q}_{\perp} E \delta c_q, \quad (\text{A.2})$$

$$(\omega - v_1 q_x) \delta c_q = v_1 c_0 \mathbf{q}_{\perp} \cdot \delta \mathbf{p}_{\perp q}. \quad (\text{A.3})$$

The dispersion relation for twist-bend modes is same as Eq. (15) because the terms containing concentration fluctuations in Eqs. (A.1) and (A.2) point in the direction of \mathbf{q}_\perp . The splay-bend modes couple to the concentration fluctuations and are obtained by taking in-plane divergence ($\nabla_\perp \cdot$) on Eqs. (A.1) and (A.2). They have the following dispersion:

$$\omega_1 = \frac{2}{3}v_0q\cos\phi - \frac{i}{3}(\nu + \Gamma K)q^2 + \frac{2^{1/3}F_1}{\left[3(F_2 + \sqrt{4F_1^3 + F_2^2})^{1/3}\right]} - \frac{(F_2 + \sqrt{4F_1^3 + F_2^2})^{1/3}}{(3 \times 2^{1/3})}, \quad (\text{A.4})$$

$$\omega_2 = \frac{2}{3}v_0q\cos\phi - \frac{i}{3}(\nu + \Gamma K)q^2 - \frac{(1 + i\sqrt{3})F_1}{\left[3 \times 2^{2/3}(F_2 + \sqrt{4F_1^3 + F_2^2})^{1/3}\right]} + \frac{(1 - i\sqrt{3})}{6 \times 2^{1/3}}(F_2 + \sqrt{4F_1^3 + F_2^2})^{1/3}, \quad (\text{A.5})$$

$$\omega_3 = \frac{2}{3}v_0q\cos\phi - \frac{i}{3}(\nu + \Gamma K)q^2 - \frac{(1 - i\sqrt{3})F_1}{\left[3 \times 2^{2/3}(F_2 + \sqrt{4F_1^3 + F_2^2})^{1/3}\right]} + \frac{(1 + i\sqrt{3})}{6 \times 2^{1/3}}(F_2 + \sqrt{4F_1^3 + F_2^2})^{1/3}, \quad (\text{A.6})$$

where $F_1 = C_1q^2 + C_2q^3 + C_3q^4$ and $F_2 = C_4q^3 + C_5q^4 + C_6q^5 + C_7q^6$. The coefficient C_i s are:

$$\begin{aligned} C_1 &= \frac{1}{2} [3\sigma_0c_0\cos 2\phi(1 + \lambda\cos 2\phi) - 6Ec_0v_0\sin^2\phi - 2v_0^2\cos^2\phi], C_2 = iv_0(\Gamma K - 2\nu)\cos\phi, \\ C_3 &= \nu^2 + \Gamma K^2 - \nu\Gamma K - \frac{3K}{4} [1 + \lambda\cos 2\phi(2 + \lambda\cos 2\phi)], \\ C_4 &= \frac{1}{2}v_0\cos\phi [4v_0^2\cos^2\phi + 9c_0(-4Ev_0\sin^2\phi - 3\sigma_0\sin^2\phi(1 + \lambda\cos 2\phi) - \sigma_0\cos 2\phi(1 + \lambda\cos 2\phi))], \\ C_5 &= \frac{-3i}{4} [4v_0^2\cos^2\phi(\Gamma K - 2\nu) + 3c_0(-4Ev_0\sin^2\phi(\Gamma K + 2\nu) + \sigma_0(\nu + \Gamma K)(\lambda + 2\cos 2\phi + \lambda\cos 4\phi))], \\ C_6 &= \frac{-3v_0}{4}\cos\phi [8\nu^2 - 4\Gamma K^2 - 8\Gamma K\nu + 3K(\lambda^2 + 5 + \lambda(7\cos 2\phi + \lambda\cos 4\phi))], \text{ and} \\ C_7 &= \frac{-i(\nu + \Gamma K)}{8} [16\nu^2 + 16\Gamma K^2 - 40\nu\Gamma K - 9K(\lambda^2 + 2 + \lambda(4\cos 2\phi + \lambda\cos 4\phi))]. \end{aligned}$$

In Fig. 7 The dotted line shows the most unstable splay-bend mode without concentration dependence, obtained from Eq. (14), whereas the dashed line shows the same as obtained from Eqs. (A.4), (A.5) and (A.6). These

two dispersion curves are essentially identical. Hence we conclude that concentration fluctuations do not alter our basic results.

-
- [1] S. Ramaswamy, *The mechanics and statistics of active matter*, Annu. Rev. Condens. Matter Phys. **1**, 323 (2010).
 - [2] M. C. Marchetti, J. F. Joanny, S. Ramaswamy, T. B. Liverpool, J. Prost, M. Rao, and R. A. Simha, *Hydrodynamics of soft active matter*, Rev. Mod. Phys. **85**, 1143 (2013).
 - [3] H. H. Wensink, J. Dunkel, S. Heidenreich, K. Drescher, R. E. Goldstein, H. Löwen, and J. M. Yeomans, *Meso-scale turbulence in living fluids*, Proc. Natl. Acad. Sci. U. S. A. **109**, 14308 (2012).
 - [4] T. Vicsek, A. Czirók, E. Ben-Jacob, I. Cohen, and O. Shochet, *Novel type of phase transition in a system of self-driven particles*, Phys. Rev. Lett. **75**, 1226 (1995).
 - [5] J. Toner and Y. Tu, *Long-range order in a two-dimensional dynamical XY model: How birds fly together*, Phys. Rev. Lett. **75**, 4326 (1995).
 - [6] J. Toner, Y. Tu, and S. Ramaswamy, *Hydrodynamics and phases of flocks*, Ann. Physics **318**, 170 (2005).
 - [7] R. Aditi Simha and S. Ramaswamy, *Hydrodynamic fluctuations and instabilities in ordered suspensions of self-propelled particles*, Phys. Rev. Lett. **89**, 058101 (2002).
 - [8] R. Voituriez, J. F. Joanny, and J. Prost, *Spontaneous flow transition in active polar gels*, Europhys Lett. **70**, 404 (2005).

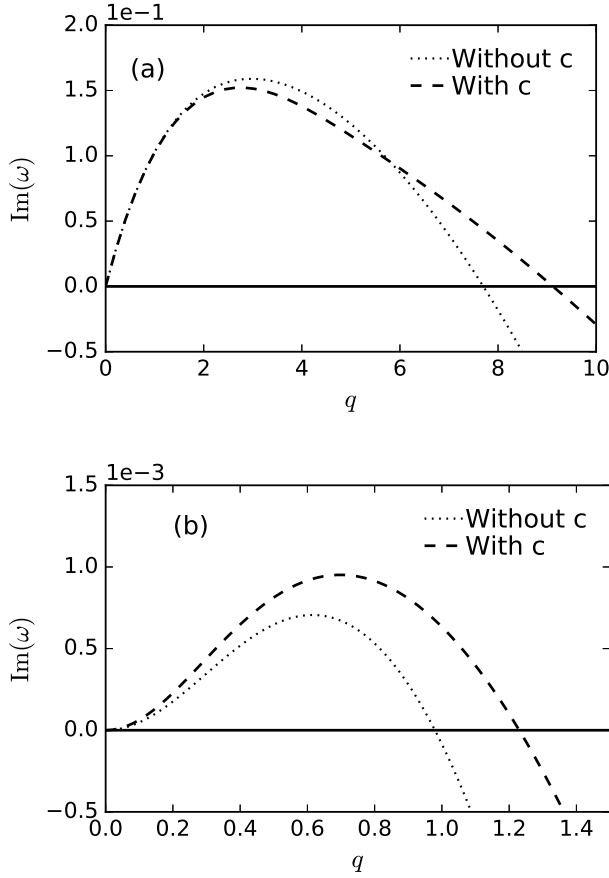


FIG. 7. Comparison of the splay-bend growth rates with and without explicit concentration dependence for (a) $O(q)$: $R = 0.1$, and (b) $O(q^2)$: $R = 5$ regimes. The other parameters are: $\phi = 15^\circ$, $\nu = 10^{-1}$, $\Gamma K = 10^{-3}$, $\lambda = 0.1$, $E = 0.05$.

[9] V. V. Fréedericksz and A. Repiewa, *Theoretisches und experimentelles zur frage nach der natur der anisotropen flüssigkeiten*. Z. Physik. **42**, 532 (1927).
 [10] P. de Gennes and J. Prost, *The Physics of Liquid Crystals*, International series of monographs on physics (Clarendon Press, 1993).
 [11] B. Martínez-Prat, J. Ignés-Mullol, J. Casademunt, and F. Sagués, *Selection mechanism at the onset of active turbulence*, Nat. Phys. **15**, 362 (2019).
 [12] G. Duclos, C. Blanch-Mercader, V. Yashunsky, G. Salbreux, J. F. Joanny, J. Prost, and P. Silberzan, *Spontaneous shear flow in confined cellular nematics*, Nat. Phys. **14**, 728 (2018).
 [13] D. Saintillan, *Rheology of active fluids*, Annu. Rev. Fluid Mech. **50**, 563 (2018).
 [14] L. Giomi and M. C. Marchetti, *Polar patterns in active fluids*, Soft Matter **8**, 129 (2012).
 [15] L. Giomi, *Geometry and topology of turbulence in active nematics*, Phys. Rev. X **5**, 031003 (2015).
 [16] J. Urzay, A. Doostmohammadi, and J. Yeomans, *Multi-scale statistics of turbulence motorized by active matter*, J. Fluid Mech. **822**, 762773 (2017).
 [17] E. Lauga and R. E. Goldstein, *Dance of the microswim-*

mers, Phys. Today **65**, 30 (2012).
 [18] K. Kruse, J. F. Joanny, F. Jülicher, J. Prost, and K. Sekimoto, *Asters, vortices, and rotating spirals in active gels of polar filaments*, Phys. Rev. Lett. **92**, 078101 (2004).
 [19] L. Giomi, M. J. Bowick, X. Ma, and M. C. Marchetti, *Defect annihilation and proliferation in active nematics*, Phys. Rev. Lett. **110**, 228101 (2013).
 [20] K. Gowrishankar and M. Rao, *Nonequilibrium phase transitions, fluctuations and correlations in an active contractile polar fluid*, Soft Matter **12**, 2040 (2016).
 [21] J. Elgeti, M. E. Cates, and D. Marenduzzo, *Defect hydrodynamics in 2d polar active fluids*, Soft Matter **7**, 3177 (2011).
 [22] A. Doostmohammadi, T. N. Shendruk, K. Thijssen, and J. Yeomans, *Onset of meso-scale turbulence in living fluids*, Nat. Commun. (2016).
 [23] S. P. Thampi, R. Golestanian, and J. M. Yeomans, *Vorticity, defects and correlations in active turbulence*. Phil. Trans. R. Soc. A **372**, 20130366 (2014).
 [24] L. Giomi, M. J. Bowick, P. Mishra, R. Sknepnek, and M. C. Marchetti, *Defect dynamics in active nematics*, Phil. Trans. R. Soc. A **372**, 20130365 (2014).
 [25] T. Sanchez, D. T. N. Chen, S. Decamp, M. Heymann, and Z. Dogic, *Spontaneous motion in hierarchically assembled active matter*, Nature **491** (2012).
 [26] S. Decamp, G. Redner, A. Baskaran, M. Hagan, and Z. Dogic, *Orientational order of motile defects in active nematics*, Nat. Mater. **14** (2015).
 [27] C. Dombrowski, L. Cisneros, S. Chatkaew, R. E. Goldstein, and J. O. Kessler, *Self-concentration and large-scale coherence in bacterial dynamics*, Phys. Rev. Lett. **93**, 098103 (2004).
 [28] T. Ishikawa, N. Yoshida, H. Ueno, M. Wiedeman, Y. Imai, and T. Yamaguchi, *Energy transport in a concentrated suspension of bacteria*, Phys. Rev. Lett. **107**, 028102 (2011).
 [29] A. Sokolov and I. S. Aranson, *Physical properties of collective motion in suspensions of bacteria*, Phys. Rev. Lett. **109**, 248109 (2012).
 [30] J. Dunkel, S. Heidenreich, K. Drescher, H. H. Wensink, M. Bär, and R. E. Goldstein, *Fluid dynamics of bacterial turbulence*, Phys. Rev. Lett. **110**, 228102 (2013).
 [31] V. Bratanov, F. Jenko, and E. Frey, *New class of turbulence in active fluids*, Proc. Natl. Acad. Sci. **112**, 15048 (2015).
 [32] Neither polar order [7] nor polar active stress [39, 43] alters the fundamental mechanism in the Stokesian limit.
 [33] N. G. Chisholm, D. Legendre, E. Lauga, and A. S. Khair, *A swimmer across reynolds numbers*, J. Fluid Mech. **796**, 233256 (2016).
 [34] S. Wang and A. M. Ardekani, *Unsteady swimming of small organisms*, J. Fluid Mech. **702**, 286297 (2012).
 [35] G. Li, A. Ostace, and A. M. Ardekani, *Hydrodynamic interaction of swimming organisms in an inertial regime*, Phys. Rev. E **94**, 053104 (2016).
 [36] T. Dombrowski, S. K. Jones, G. Katsikis, A. P. S. Bhalla, B. E. Griffith, and D. Klotsa, *Transition in swimming direction in a model self-propelled inertial swimmer*, Phys. Rev. Fluids **4**, 021101 (2019).
 [37] D. Klotsa, K. A. Baldwin, R. J. A. Hill, R. M. Bowley, and M. R. Swift, *Propulsion of a two-sphere swimmer*, Phys. Rev. Lett. **115**, 248102 (2015).
 [38] N. Riley, *On a sphere oscillating in a viscous fluid*, Quart. Journ. Mech. and Applied Math. **19**, 461 (1966).

- [39] L. Giomi, M. C. Marchetti, and T. B. Liverpool, *Complex spontaneous flows and concentration banding in active polar films*, Phys. Rev. Lett. **101**, 198101 (2008).
- [40] G. d'Étude des cristaux liquides Orsay, *Dynamics of fluctuations in nematic liquid crystals*, J. Chem. Phys. **51**, 816 (1969).
- [41] E. M. Purcell, *Life at low reynolds number*, Am. J. Phys. **45**, 3 (1977).
- [42] W. Kung, M. Cristina Marchetti, and K. Saunders, *Hydrodynamics of polar liquid crystals*, Phys. Rev. E **73**, 031708 (2006).
- [43] M. C. Marchetti and T. N. Liverpool, in *Cell Motility*, edited by P. Lenz (Springer-Verlag, Berlin, 2007).
- [44] A. Maitra, P. Srivastava, M. C. Marchetti, S. Ramaswamy, and M. Lenz, *Swimmer suspensions on substrates: anomalous stability and long-range order*, arXiv:1901.01069.
- [45] K. Kruse, J. F. Joanny, F. Jülicher, J. Prost, and K. Sekimoto, *Generic theory of active polar gels: a paradigm for cytoskeletal dynamics*, Eur. Phys. J. E **16**, 516 (2005).
- [46] We assume concentrations are high enough that F globally favours a nonzero magnitude for \mathbf{p} . We therefore ignore c -dependence in the polynomial part of F .
- [47] F. C. Frank, *I. liquid crystals. on the theory of liquid crystals*, Discuss. Faraday Soc. **25**, 19 (1958).
- [48] H. Zocher, *The effect of a magnetic field on the nematic state*, Trans. Faraday Soc. **29**, 945 (1933).
- [49] C. W. Oseen, *The theory of liquid crystals*, Trans. Faraday Soc. **29**, 883 (1933).
- [50] D. Forster, *Microscopic theory of flow alignment in nematic liquid crystals*, Phys. Rev. Lett. **32**, 1161 (1974).
- [51] H. Stark and T. C. Lubensky, *Poisson-bracket approach to the dynamics of nematic liquid crystals*, Phys. Rev. E **67**, 061709 (2003).
- [52] N. Kumar, H. Soni, S. Ramaswamy, and A. Sood, *Flocking at a distance in active granular matter*, Nat. Commun. **5** (2014).
- [53] M. C. Marchetti, personal communication.
- [54] Formally we could justify this neglect by introducing birth and death so that the concentration becomes a fast variable; see John Toner - *Birth, Death and Flight: A Theory of Malthusian Flocks*, Phys. Rev. Lett., **108**, 088102 (2012).
- [55] In molecular or colloidal systems $\mu/\rho \gg K/\mu$. Assuming this inequality holds for the systems of interest here as well, G and \bar{G} are uniformly negative.
- [56] A. M. Leshansky and O. Kenneth, *Surface tank treading: propulsion of Purcells toroidal swimmer*, Phys. Fluids **20**, 063104 (2008).
- [57] Even for slow swimmers, one could imagine inertia, in the form of R , overcoming the force-dipole instability in the case of a swimmer with a small dipole (and hence a small σ_0), propelled mainly by its quadrupole force moment.
- [58] T. N. Shendruk, K. Thijssen, J. M. Yeomans, and A. Doostmohammadi, *Twist-induced crossover from two-dimensional to three-dimensional turbulence in active nematics*, Phys. Rev. E **98**, 010601 (2018).
- [59] C. Canuto, M. Y. Hussaini, A. Quarteroni, and T. A. Zang, eds., *Spectral Methods in Fluid Dynamics*, Springer Series in Computational Physics (Springer, New York, 1988).
- [60] S. Cox and P. Matthews, *Exponential time differencing for stiff systems*, J. Comput. Phys. **176**, 430 (2002).
- [61] D. Egolf and H. Greenside, *Characterization of the transition from defect to phase turbulence*, Phys. Rev. Lett. **74**, 1751 (1994).
- [62] C. Jayaprakash, F. Hayot, and R. Pandit, *Universal properties of the two-dimensional Kuramoto-Sivashinsky equation*, Phys. Rev. Lett. **71**, 12 (1993).
- [63] H. Chaté and P. Manneville, “Phase Turbulence” in *Turbulence, P. Tabeling & O. Cardoso, eds.*, (NATO ASI Series B: Physics, v. 341, Springer, Boston, MA, 1995).
- [64] The value of ξ obtained from the fit is comparable to the one obtained using the definition $\xi \equiv \int_0^{L/2} C(r)dr$.
- [65] We have verified that the results of our DNS do not change if the advective nonlinear term in Eq. (4) is absent.
- [66] L. M. Smith and W. C. Reynolds, *The dissipation-range spectrum and the velocity-derivative skewness in turbulent flows*, Phys. Fluids A **3** (1991).
- [67] U. Frisch, *Turbulence: The Legacy of A. N. Kolmogorov* (Cambridge University Press, 1995).